

JOURNAL ARTICLE

Rician likelihood loss for quantitative MRI using self-supervised deep learning

Christopher S. Parker¹  | Anna Schroder¹  | Sean C. Epstein¹  | James Cole¹  | Daniel C. Alexander¹  | Hui Zhang¹ 

¹Centre for Medical Image Computing,
University College London, London,
United Kingdom

Correspondence

Christopher S. Parker, CMIC, 90 High
Holborn, London, WC1V 6LJ. Email:
christopher.parker@ucl.ac.uk

Funding Information

CSP, DCA and HZ are supported
by the Medical Research Council;
grant MR/T046473/1. AS is
supported by the EPSRC funded
i4health CDT; grant EP/S021930/1.
SCE is supported by the EPSRC-
funded UCL Centre for Doctoral
Training in Medical Imaging; grant
EP/L016478/1.

ABSTRACT

Purpose: Previous quantitative MR imaging studies using self-supervised deep learning have reported biased parameter estimates at low SNR. Such systematic errors arise from the choice of Mean Squared Error (MSE) loss function for network training, which is incompatible with Rician-distributed MR magnitude signals. To address this issue, we introduce the negative log Rician likelihood (NLR) loss.

Methods: A numerically stable and accurate implementation of the NLR loss was developed to estimate quantitative parameters of the apparent diffusion coefficient (ADC) model and intra-voxel incoherent motion (IVIM) model. Parameter estimation accuracy, precision and overall error were evaluated in terms of bias, variance and root mean squared error and compared against the MSE loss over a range of SNRs (5 – 30).

Results: Networks trained with NLR loss show higher estimation accuracy than MSE for the ADC and IVIM diffusion coefficients as SNR decreases, with minimal loss of precision or total error. At high effective SNR (high SNR and small diffusion coefficients), both losses show comparable accuracy and precision for all parameters of both models.

Conclusion: The proposed NLR loss is numerically stable and accurate across the full range of tested SNRs and improves parameter estimation accuracy of diffusion coefficients using self-supervised deep learning. We expect the development to benefit quantitative MR imaging techniques broadly, enabling more accurate parameter estimation from noisy data.

KEYWORDS:

Quantitative MRI, Rician, Self-supervised, Likelihood

1 | INTRODUCTION

Quantitative MRI (qMRI) aims to estimate and map tissue properties of interest using biophysical models that relate these properties, as parameters, to measured MR signals^{1,2}. Such parameter estimation enables the assessment of the spatial and subject-wise variability in target tissue properties, which can inform understanding of disease processes and support objective, data-driven evaluation of patients from MRI data. For reliable inference and interpretation of tissue properties with qMRI, accurate parameter estimation is essential.

Biophysical model parameters are traditionally estimated by optimising a fitting objective function for each voxel of an MR image. This can be time-consuming, taking minutes to hours for a single volume. Furthermore, for complex non-linear models with many parameters, the objective function is often non-convex and contains local minima, increasing the propensity for estimation errors.

Deep learning approaches, which predict the model parameters directly from measured MR data have been developed to overcome some of these limitations, demonstrating orders-of-magnitude improvement in inference speed and more robust parameter estimates^{3,4,5,6,7,8,9}. These can be divided into two categories: supervised and self-supervised. Supervised approaches aim to minimise the difference between the parameter estimates and the parameter gold standards (or ground truths) that accompany the MR data. Self-supervised approaches instead minimise a measure of loss between the signal predictions under the parameter estimates and the MR data. Supervised approaches were developed first³, but have been shown to produce significantly biased estimates^{6,10}. Self-supervised approaches were in part motivated to overcome this issue⁴. However, studies using self-supervised learning show that bias in the estimated model parameters persists at low SNR^{4,5,7}.

The reported bias can be explained by the choice of network training loss function. So far, self-supervised networks have been trained using the Mean Squared Error (MSE) loss^{4,5,6,7,8,11,12,9}. This is the standard way to quantify reconstruction error in self-supervised settings¹³. Minimising the MSE is equivalent to least squares estimation, which is unbiased only if the noise is centered on the true signal i.e., has zero mean^{14,15,16}. However, MR magnitude signals used in qMRI follow a Rician distribution with non-zero mean noise¹⁷. This violation of the least squares assumption may result in biased parameter estimates.

To address this, we propose a negative log Rician likelihood loss function for network training in self-supervised qMRI. Training then becomes analogous to maximum likelihood estimation (MLE), which is known to be asymptotically unbiased^{18,19}. Although previous studies have recognised the need for a Rician likelihood-based loss when training self-supervised networks on MR magnitude images^{20,21}, none

have so far demonstrated a numerically stable and accurate implementation.

In this study, we describe the theoretical basis for parameter estimation bias when using the MSE loss for self-supervised qMRI. We next introduce a numerically stable and accurate implementation of the negative log Rician likelihood loss. We then empirically evaluate the accuracy and precision of the proposed loss function using the apparent diffusion coefficient (ADC) model and intra-voxel incoherent motion (IVIM) model as example applications. Results show improved parameter estimation accuracy at low SNR with minimal loss of precision.

2 | THEORY

2.1 | Self-supervised quantitative MRI

qMRI estimates the parameters of a biophysical model of the MR signal from a set of measured signals acquired in an image voxel. The measured signals are acquired under varying experimental conditions to provide contrast for parameter estimation and are equal or larger in number than the set of model parameters.

In self-supervised qMRI, a neural network is trained to predict parameters directly from a set of signal measures by minimising a measure of error between the noise-free signals predicted by the model parameters and the measured signals. This architecture mimics that of an autoencoder¹³, with the input being the measured signals, the encoder being a fully connected neural network, the latent space being the model parameters, and the decoder being the biophysical model (Fig. 1).

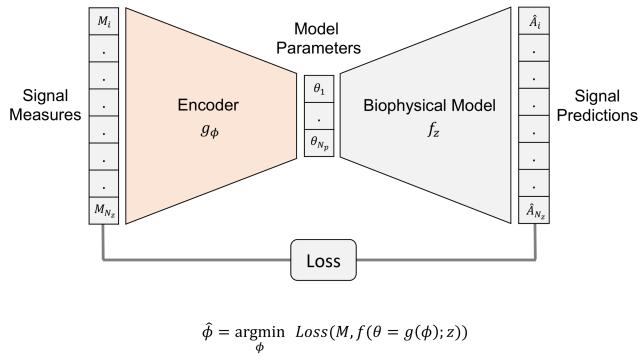
2.2 | Mean squared error loss function

Self-supervised neural networks are trained to minimise an amortised loss, which is the average of some measure of error between signal measures and signal predictions over a set of voxels. The MSE loss function, denoted L_{MSE} , trains networks to minimise the mean squared error between the predicted and measured MR signals, and is calculated as:

$$L_{MSE} = \frac{1}{N} \sum_{j=1}^N \left[\frac{1}{N_z} \sum_{i=1}^{N_z} (M_{i,j} - \hat{A}_{i,j})^2 \right] \quad (1)$$

where M is the measured signal, \hat{A} is the predicted signal, N_z is the number of measured signals in a voxel and N is the number of voxels in the batch. The set of signal measures in a voxel, $\{M_i | i = 1, \dots, N_z\}$, are acquired under varying experimental conditions $\{z_i | i = 1, \dots, N_z\}$ and the set of corresponding signal predictions, $\{\hat{A}_i = f(\theta; z_i) | i =$

a. Self-supervised qMRI



b. Autoencoder

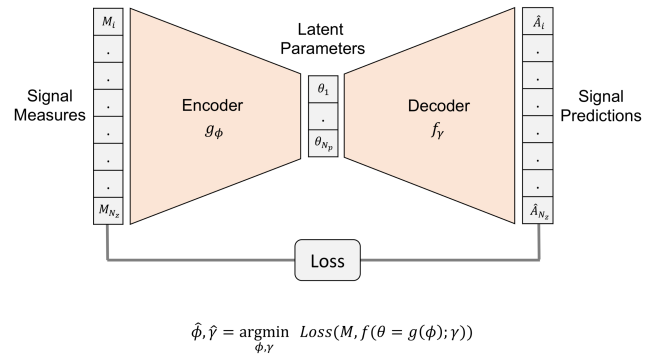


FIGURE 1 Comparison between self-supervised qMRI and autoencoders in terms of network architecture and optimisation. The shaded orange region denotes the trained component of the architecture. **a.** Self-supervised qMRI. The encoder network parameters are trained to output the model parameters that minimise the loss between the signal measures and the signal predictions. Signal predictions are made under the model parameters and the corresponding biophysical model. **b.** Autoencoders. The encoder and decoder network parameters are trained to minimise the loss between the signal measures and the signal predictions. Signal predictions are made under the encoded latent space parameters via the decoder.

$1, \dots, N_z\}$, are generated from the chosen biophysical model with model parameters θ .

The global minimum of the MSE loss function occurs when the least squares estimate of the signal predictions are attained for each voxel. Least squares predictions closely match the measured data and are unbiased estimates of the noise-free signal when the noise distribution has zero mean i.e., is centered on the noise-free signal^{14,15,16}. Hence, least squares predictions are maximum likelihood estimates under the assumption of zero-mean Gaussian noise²². However, in qMRI, magnitude signal measures are typically used, which are neither Gaussian nor centered on the noise-free signal.

2.3 | MR magnitude signals

The raw MR signal consists of a real and imaginary component, each of which is corrupted by zero-mean Gaussian noise. Magnitude signals are commonly calculated for quantitative MR imaging as they avoid phase artifacts. The magnitude of the complex-valued signal, $M = \sqrt{N_R^2 + N_I^2}$, where N_R and N_I are real Gaussian-distributed random variables representing the real and imaginary components, follows a Rician distribution¹⁷ with probability density function:

$$p(M|A, \sigma) = \frac{M}{\sigma^2} e^{-\frac{(M^2 + A^2)}{2\sigma^2}} I_0\left(\frac{MA}{\sigma^2}\right) \quad (2)$$

where I_0 is the modified Bessel function of the first kind with order zero, A is the true noise-free signal that the biophysical model aims to predict, and σ is the noise standard deviation. The centre of this distribution, $E[M|A, \sigma]$, corresponding to the expected least squares estimate of A , is always greater than A :

$$E[M|A, \sigma] = \sigma \sqrt{\frac{\pi}{2}} L_{\frac{1}{2}}\left(\frac{-A^2}{2\sigma^2}\right) > A \quad (3)$$

where $L_{1/2}$ is the Laguerre polynomial. The lower the SNR, the greater the difference between A and the least squares estimate (Fig. 2).

Fig. 2 and Eq. (3) show that, with sufficient degrees of freedom, signal predictions from biophysical models can lower MSE by predicting signals that are higher than the true noise-free signal. In this case the signal prediction and associated model parameter estimates are biased. Using the MSE

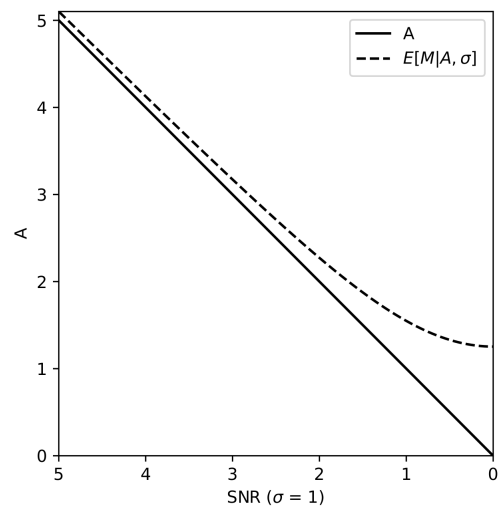


FIGURE 2 The expected value of the measured signal, $E[M|A, \sigma]$, as a function of SNR. $E[M|A, \sigma]$ corresponds to the centre of the noise and the least squares estimate of the noise-free signal at a particular SNR. Its value increasingly overestimates A as SNR decreases.

loss for self-supervised quantitative MR imaging is therefore likely to be a source of bias in parameter estimates.

2.4 | Rician likelihood loss function

An alternative method for parameter estimation is MLE. MLE aims to maximise the probability of the measured data under the predicted signal and noise. This method is known to be statistically consistent, in that it is asymptotically unbiased when the model noise distribution matches that of the measured data^{18,19}. An equivalent way to justify unbiasedness of MLE is that its predictive distribution is as close as possible to the empirical data distribution²². As MR signals are Rician-distributed, a Rician likelihood loss function may be optimised in self-supervised quantitative MR imaging to provide unbiased parameter estimates.

The Rician likelihood of a predicted signal is given by Eq. (2). Assuming each MR measure in a voxel is independent, the total likelihood across all signal predictions for a voxel is the product of likelihoods. Network training involves minimising a loss function; in this context, Rician likelihood may be maximised by defining the training loss as the negative of the Rician likelihood. The Rician likelihood, R , defined for a single voxel is:

$$R = \prod_{i=1}^{N_z} p(M_i | \hat{A}_i, \sigma) \quad (4)$$

As a joint probability, Eq. (4) is subject to numerical overflow because it requires taking the product of multiple probabilities. It is common therefore to instead minimise the negative of the logarithm of the Rician likelihood. The log transformation turns multiplication into summation, reducing its propensity to overflow. Being a positively monotonic function, the log transformation preserves the location of the losses global minimum. The negative of the log Rician likelihood for a voxel is:

$$-\log(R) = -\sum_{i=1}^{N_z} \log\left(\frac{M_{i,j}}{\sigma^2}\right) - \frac{M_{i,j}^2 + \hat{A}_{i,j}^2}{2\sigma^2} + \log\left(I_0\left(\frac{M_{i,j}\hat{A}_{i,j}}{\sigma^2}\right)\right) \quad (5)$$

2.5 | Loss function specification - practical challenges

Implementing Eq. (5) in practice is non-trivial. A naïve implementation, which directly programmes the equation as specified, has been found to be numerically unstable²¹. Our own evaluation suggests this is because $\log(I_0(x))$ and its gradient both contain modified Bessel functions, which grow exponentially with the input value.

To overcome this, several approaches that avoid the direct computation of $I_0(x)$ have been reported^{23,24,20} (Table S1).

We have found that none so far provide satisfactory performance in terms of both accuracy and stability across a wide range of SNRs (Fig. S1, Table S2). The approach based on log-sum-exp²⁰ has poor accuracy at high SNR; this may be improved but at the cost of significantly longer computation time. Hankel’s and related approximations^{23,24} have poor accuracy at low SNR. Furthermore, we have found that both are subject to overflow.

$$I_0^e(x) = e^{-x} I_0(x) := \begin{cases} e^{-x} [e^x P_L(x)] = P_L(x) = \sum_{i=0}^{30} c_i^L T_i(x_t), & \text{if } 0 \leq x \leq 8 \\ e^{-x} [e^x P_H(x) / \sqrt{x}] = P_H(x) / \sqrt{x} = \sum_{i=0}^{25} c_i^H T_i(x_t) / \sqrt{x}, & \text{if } 8 < x < \infty \end{cases} \quad (6)$$

The coefficients are tailored for high accuracy over low and high input ranges. x_t is x transformed to the range $[-1, 1]$ over which the Chebyshev polynomials are defined. The transformations and coefficients are given in www.netlib.org/cephes²⁵.

As shown in Eq. (6), the exponentially scaled Bessel function is simply the $I_0(x)$ approximation with the exponential term removed. As $\log(I_0^e(x)) = \log(I_0(x)) - x$, then a numerically stable computation of the log Bessel that avoids direct computation of $I_0(x)$ is $\log(I_0(x)) = \log(I_0^e(x)) + x$. This formulation can be readily implemented in common machine learning packages, for example in PyTorch using *torch.special.i0e*. The final implementation of the negative log Rician likelihood loss function (NLR) is:

$$L_{NLR} = \frac{1}{N} \sum_{j=1}^N \left[- \sum_{i=1}^{N_z} \log \left(\frac{M_{i,j}}{2\sigma^2} \right) - \frac{M_{i,j}^2 + \hat{A}_{i,j}^2}{2\sigma^2} + \log \left(I_0^e \left(\frac{M_{i,j} \hat{A}_{i,j}}{\sigma^2} \right) \right) + \frac{M_{i,j} \hat{A}_{i,j}}{\sigma^2} \right] \quad (7)$$

L_{NLR} ’s global minimum is obtained when the MLE of the model parameters are predicted for each voxel. In this case, and under asymptotic conditions (as the number of measured data approaches infinity), the negative Rician loss function will train networks to predict unbiased parameter estimates. As it is not possible to assess unbiasedness of L_{NLR} analytically for a finite number of measured signals per voxel, empirical observation using simulated data is required to assess estimation performance.

Note that the likelihood requires users to specify the value of the noise standard deviation, σ , which can be considered to be constant over voxels at a given SNR. In this work we use an unbiased method to estimate σ , although several other methods have also been proposed (see section 3.2.3).

We propose a new approach that is numerically stable and highly accurate for a wide range of SNRs and can be readily implemented in common machine learning packages (Table S1, Proposed). The approach utilises the exponentially scaled Bessel function $I_0^e(x)$ ^{25,26}, which approximates $I_0(x)$ as a weighted sum of Chebyshev polynomials, T_i , multiplied by e^x (as introduced by Blair and Edwards²⁷, Blair²⁸):

3 | METHODS

3.1 | Quantitative MR biophysical models

We investigate parameter estimation accuracy and precision for two qMRI models: the ADC model²⁹ and the intra-voxel incoherent motion (IVIM) model³⁰.

3.1.1 | ADC model

The ADC model is a simple mono-exponential signal decay model, a widely used model in diffusion imaging and across various qMRI applications, such as relaxometry. It also serves as a base for more complex qMRI models.

The ADC model attempts to capture the extent of apparent water diffusion within a voxel. By assuming isotropic and Gaussian diffusion in all directions, the diffusion-weighted signal decays monoexponentially and is parameterised by the apparent diffusion coefficient D and the signal in the absence of diffusion weighting, S_0 . The predicted MR signal, \hat{A}_{ADC} , for the ADC model is:

$$\hat{A}_{ADC} = S_0 e^{-bD} \quad (8)$$

To estimate the ADC model parameters multiple signals are acquired in a single voxel across a range of b-values. D is upper-bounded by the diffusivity of free water ($3 \mu\text{m}^2/\text{ms}$ at body temperature), with lower values indicating the presence of microstructural barriers to water diffusion (e.g., cell membranes).

3.1.2 | IVIM model

The IVIM model is to date the most widely used model for qMRI studies that use self-supervised deep learning.

The IVIM model extends the ADC model to account for incoherent motion (zero-centered displacement) of water

within capillaries. In the presence of capillary incoherent motion and isotropic Gaussian diffusion, the diffusion-weighted signal decays biexponentially and is parameterised by the diffusion coefficient of tissue D_t , pseudo-diffusion coefficient of the capillaries D_p , signal fraction of the pseudo-diffusion component f , and S_0 as defined above. The predicted MR signal, \hat{A}_{IVIM} , for the IVIM model is:

$$\hat{A}_{IVIM} = S_0 \left(f \cdot e^{-b(D_p + D_t)} + (1 - f) \cdot e^{-bD_t} \right) \quad (9)$$

As with the ADC model, to estimate the IVIM parameters, multiple signals are acquired in a single voxel across a range of b-values. As incoherent motion within capillaries is faster than diffusion, lower b-values are often acquired to capture the rapid signal decay. D_t behaves similar to D of the ADC model, but D_p , which models pseudo-diffusion due to blood flow in randomly oriented capillaries, is orders of magnitude larger than D_t . The fraction f reflects the relative volume fraction of capillaries in a voxel.

3.2 | Self-supervised neural network

3.2.1 | Network architecture

A feed-forward deep neural network was constructed in PyTorch (v 1.21.1) to estimate voxel-wise qMRI model parameters using self-supervised learning. Following Barbieri et al.⁴, the network has one input layer, three fully connected hidden layers (the encoder), and one output layer (the model parameters). Three fully connected layers has been shown to be optimal for quantitative imaging of intra-voxel incoherent motion (IVIM) parameters⁴.

The number of nodes in the input layer and in each hidden layer was equal to the number of acquired MR signals per voxel. The number of nodes in the output layer of the encoder was set equal to the number of model parameters for the corresponding quantitative MR model - two for ADC (D and S_0), or four for IVIM (D_t , D_p , f and S_0). Encoder nodes used an exponential linear unit activation function³¹. The predicted MR signal was generated from the output layer values following the corresponding qMRI model, Eq. 8 for the ADC model or Eq. 9 for the IVIM model. To output signal predictions, b-values for predicted signals were ordered identically to the b-values used to simulate the input measurements. For the backpropagation to take approximately equally sized parameter update steps, b-values were specified in units of $\text{ms}/\mu\text{m}^2$ so that the diffusion coefficient model parameter (D for ADC and D_t for IVIM) and S_0 were of the same magnitude ($0.4\text{-}2 \mu\text{m}^2/\text{ms}$ and $0\text{-}1$ a.u., respectively).

3.2.2 | Loss functions

Networks were constructed with either the negative log Rician likelihood loss function, L_{NLR} , given in Eq. (7), or the MSE loss function, L_{MSE} , given in Eq. (1).

3.2.3 | Sigma estimation

The NLR loss function requires an estimate of the noise standard deviation σ , assumed to be constant across voxels at a given SNR. In this case, σ may be estimated from a background image region where there is no signal. In such regions, the Rician distribution becomes a Rayleigh distribution, with expected mean:

$$E[M] = \sigma \sqrt{\frac{\pi}{2}} \quad (10)$$

Using the sample mean estimate of $E[M]$, an estimate of σ is:

$$\hat{\sigma} = \frac{\sum_{i=1}^{N_{BG}} M_i}{N_{BG} \sqrt{\frac{\pi}{2}}} \quad (11)$$

where N_{BG} is the number of background voxels, which in this study was set to 10,000. Sijbers et al.³² show that this estimate is unbiased. Other methods to estimate σ also exist (e.g., Sijbers et al.^{32,33}, Rajan et al.³⁴).

3.3 | Network training

3.3.1 | Simulated MR signals

Simulated MR signals were used for network training. At a given SNR (for the $b=0 \text{ ms}/\mu\text{m}^2$ signal), measured MR signals were simulated for 200,000 training voxels. Ground truth model parameter values for the training data were sampled uniformly from 10 equidistant numbers covering the range of physiologically plausible values: for the ADC model, $[0.4, 2] \mu\text{m}^2/\text{ms}$ for D and $[0.8, 1.2]$ a.u. for S_0 ; for the IVIM model, $[0.4, 2] \mu\text{m}^2/\text{ms}$ for D_t , $[10, 150] \mu\text{m}^2/\text{ms}$ for D_p , $[0.1, 0.5]$ for f and $[0.8, 1.2]$ a.u. for S_0 . For each voxel, diffusion MR signals were simulated under a range of b-values and complex Gaussian noise was added before computing the magnitude to produce Rician-distributed signal measures. For the IVIM model, ten b-values, representative of practical protocols, were chosen: 0, 10, 20, 30, 50, 80, 100, 200, 400 and $800 \text{ ms}/\mu\text{m}^2$. For the ADC model, ten b-values linearly spaced between 0 and $1000 \text{ ms}/\mu\text{m}^2$ (inclusive) were chosen to provide comparable signal coverage as the IVIM model. MR signal measures for an additional 1,000 voxels were also simulated to calculate validation loss. Data were simulated for SNRs of 30, 20, 10, 7.5 and 5. This range covers the SNRs commonly observed in real data (typically 10-30) and

includes even lower SNRs to test the limits of parameter estimation performance. Note hereafter that the unqualified term “SNR” will refer to the SNR of the signal at $b=0$ ms/ μs^2 , whereas “effective SNR” will refer to the signal acquired at a particular b -value and set of model parameter values.

3.3.2 | Optimisation

For each SNR, self-supervised network parameters were optimised to perform parameter estimation from the set of simulated MR training signals using either the NLR or MSE loss function. Network weights and biases were updated using stochastic gradient descent via backpropagation. An Adam optimiser was used with the default PyTorch settings (learning rate=0.001, betas=(0.9, 0.0999), weight decay=0)³⁵. Batch sizes of 256 voxels were used in each gradient descent step. To prevent dependence on the random initialisation of weights and biases, a common initialisation was used for both loss functions at each SNR. The common initialisation was determined as the trained network with lowest validation loss over 16 training repetitions using the NLR loss. Training was then initiated using the common initialisation for each loss function. Training was terminated if the loss function did not improve for 50 consecutive epochs or if a total of 300 training epochs were reached.

3.4 | Evaluation of parameter estimation performance

For each SNR, 200,000 unseen simulated test voxels were produced identically to the training data (i.e., uniformly sampled across the parameter space) but with different noise instantiations. The network trained at the corresponding SNR then predicted the model parameter values from the test voxel signal measures and the error was calculated (estimate minus ground truth). Parameter estimation performance was evaluated in detail at one representative low and one high SNR, and then examined across a range of SNRs.

Parameter estimation performance was evaluated at SNR=10 (representing typical low SNR) and SNR=30 (representing typical high SNR). Metrics of accuracy and precision were calculated as a function of the parameter value. For each unique parameter combination, bias (the average error) against ground truth was calculated to quantify accuracy, standard deviation was calculated to quantify precision and root mean squared error (RMSE) was calculated to report overall deviation from ground truth. To visualise these metrics and their variation for a particular parameter and parameter value, the average and standard deviation of each metric was calculated over the unique parameter combinations of the remaining parameter(s) (e.g., over the unique values of S_0 for D in the case of the ADC model).

Performance was then studied across a range of SNRs for each model parameter to observe the overall error trends and to allow for direct comparison of performance to Barbieri et al.⁴. At each SNR, the distribution of all errors across all training voxels was plotted for SNRs of 30, 20, 10, 7.5 and 5.

4 | RESULTS

4.1 | Parameter estimation performance at low SNR

At low SNR, the MSE loss showed significant bias in diffusion coefficient estimation that worsened with higher diffusion coefficients; that is – when the effective SNR (the SNR of the diffusion-weighted signal under the model parameters) was lower; with bias reaching 5% and 20% for ADC D and IVIM D_p diffusion coefficients, respectively (Fig. 3). In comparison, the NLR loss showed comparatively improved accuracy of diffusion coefficient estimation for both models, with only minor overestimation of ADC diffusion coefficient by 1% at high diffusivities.

Precision decreased and overall error increased with higher diffusivity for both losses, as shown by increasing standard deviation and RMSE. Both losses performed equally well in terms of accuracy, precision and overall deviation from ground truth for the D_p and f IVIM parameters. Interestingly, both losses showed relatively worse accuracy for IVIM D_p and f than for D_t .

4.2 | Parameter estimation performance at high SNR

At high SNR, both losses showed improved accuracy and precision. However, even at high SNR, the MSE loss showed systematic underestimation of ADC diffusion coefficient D as diffusivity increased (effective SNR decreased, Fig. 4, upper left), with bias reaching 1% at high diffusivities. In comparison, the NLR loss showed no significant bias in ADC diffusion coefficient estimation at high SNR. Accuracy of the IVIM model parameters D_t , D_p and f was approximately equal for MSE and NLR losses. Precision and overall deviation from ground truth was also approximately equal and generally increased with higher parameter values (lower effective SNR) for both ADC and IVIM model parameters.

4.3 | Error distribution across SNRs

The summary of errors across SNRs shows similar trends to that observed at the representative high and low SNRs in Fig. 3 and 4. Boxplots show the MSE loss tended to underestimate the ADC and IVIM diffusion coefficient as SNR decreased

(median lower than zero, Fig. 5). In comparison, the NLR loss showed a relatively more stable accuracy as SNR decreased.

As SNR decreased, both losses showed a reduction in precision (wider interquartile range) for all metrics, with the NLR

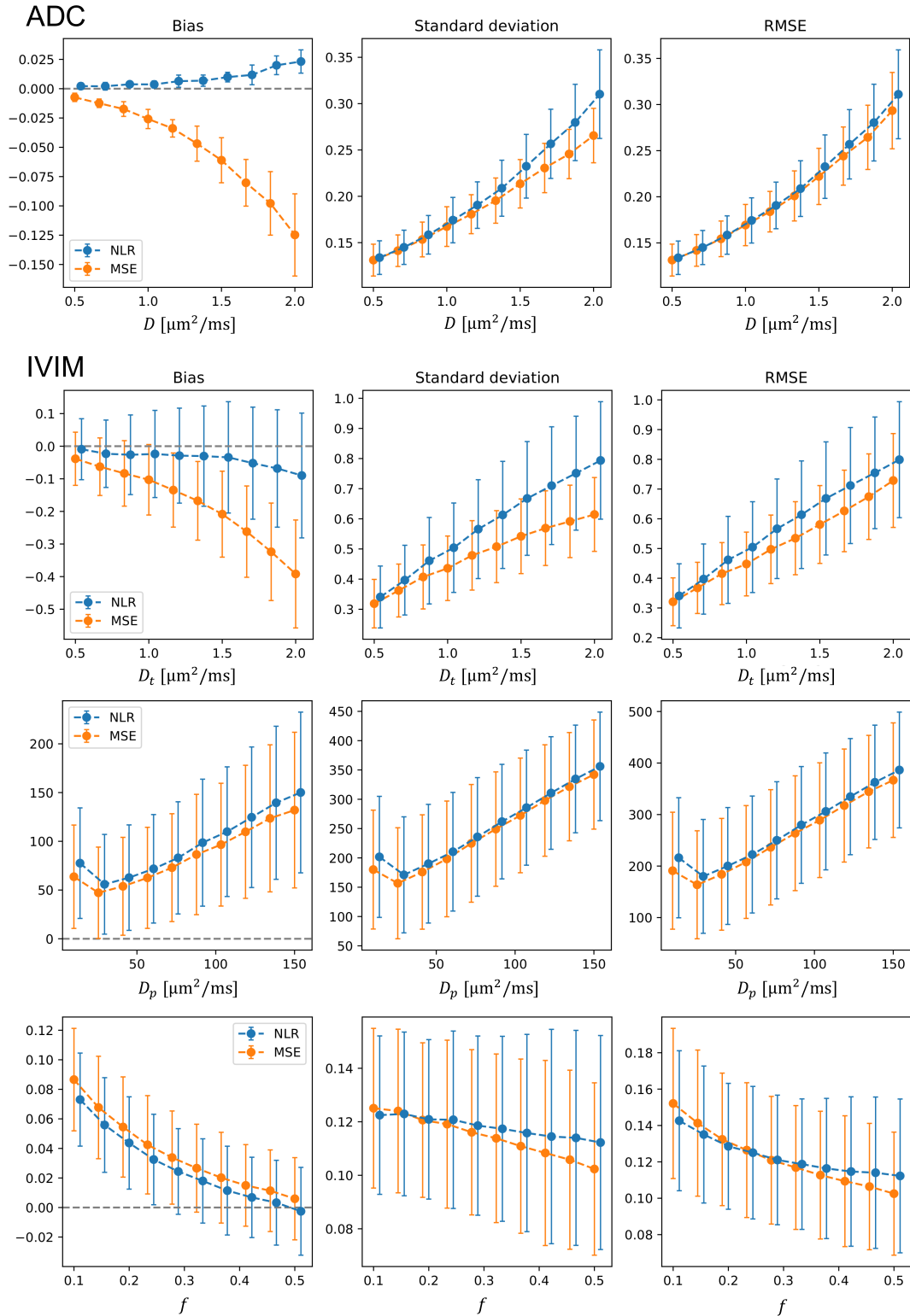


FIGURE 3 Comparison of estimation performance at a low SNR of 10 between self-supervised networks trained with NLR or MSE loss for ADC and IVIM model parameters. Points and error bars correspond to the mean and standard deviation of the performance metric across unique parameter values. NLR points and error bars have been offset to the right to aid visualisation.

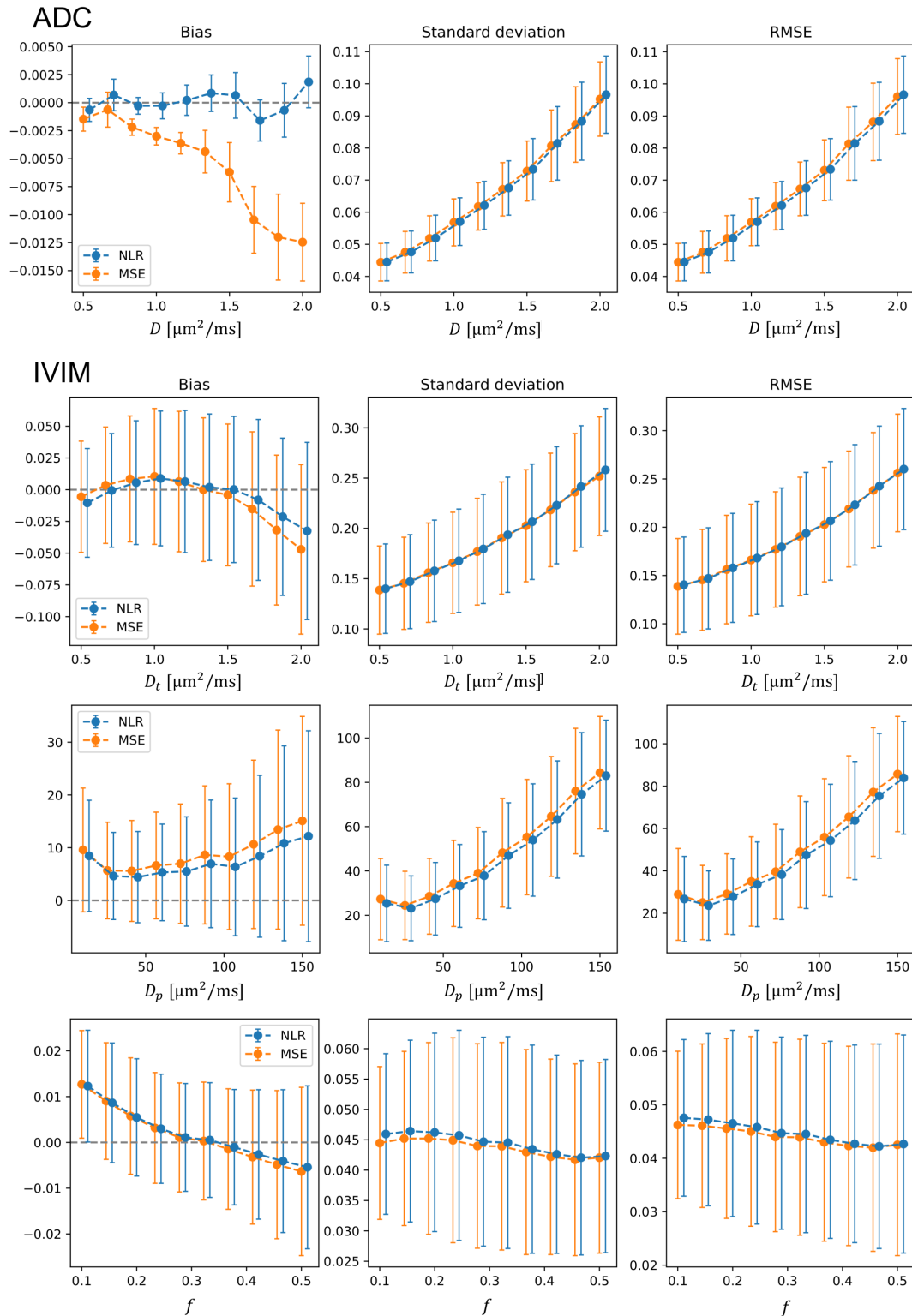


FIGURE 4 As in Fig. 3 but for a high SNR of 30.

loss showing marginally lower precision than the MSE loss. Furthermore, both losses showed increasing overestimation of IVIM f as SNR decreased. At high SNR (>10), both losses showed comparable error distributions.

5 | DISCUSSION

Previous qMRI studies using self-supervised deep learning have demonstrated increasingly biased parameter estimates at

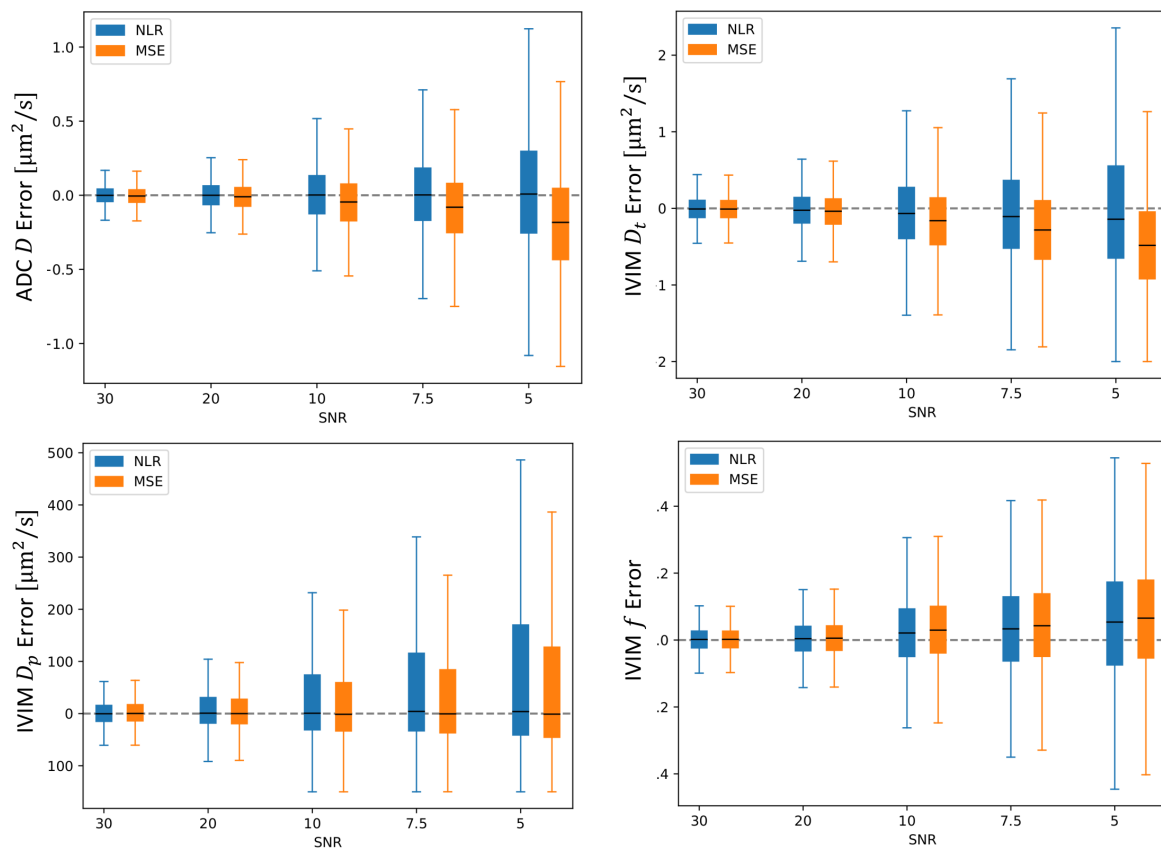


FIGURE 5 Boxplots of errors for ADC D and IVIM D_t , D_p and f model parameters at SNRs of 30, 20, 10, 7.5 and 5. The line shows the median error across all estimates and the box shows the inter-quartile range. Whiskers extend to the most extreme data point within 1.5 times the inter-quartile range from the median.

low SNR. This work suggests that a major source of bias is the use of MSE loss function, the assumptions of which are increasingly violated as SNR decreases. To overcome this, we propose and evaluate a numerically stable negative log Rician likelihood loss function for self-supervised training. Using the ADC and IVIM models as exemplars, use of NLR loss improves estimation accuracy of diffusion coefficients as SNR decreases, with none or minimal loss of precision.

We propose a novel robust computational implementation of the Rician log-likelihood loss function for self-supervised training. The implementation computes the log-Bessel using the exponentially-scaled Bessel function, resulting in high numerical stability, while its approximation using Chebyshev polynomials is highly accurate (Fig. S1). This permits calculation of the Rician log-likelihood over the full range of SNRs encountered in practical diffusion MR imaging scenarios. On the other hand, previous implementations were found to be either inaccurate or numerically unstable for these SNR ranges. Recently, Simpson et al.²⁰ proposed an approximation of the Rician log-likelihood for self-supervised learning based on finite series summation and applied this to image registration. However, as described in section 2.5, this finite series

implementation is inaccurate at high SNR and was found to be numerically unstable at very low SNR (<5).

Both loss functions demonstrated high estimation accuracy at high effective SNR – when the SNR was high and the model parameters resulted in relatively low signal attenuation (i.e., at small diffusion coefficients). Under these conditions, the Rician distribution is well approximated by a Gaussian and the center of the measured data, corresponding to the least squares signal prediction, is closer to the true noise-free signal. It should be noted however that even at high SNR the MSE loss can produce biased estimates when the effective SNR is low – at high SNR, as the diffusion coefficient increases, estimation accuracy becomes comparably worse for the MSE loss than the NLR loss (Fig. 4). MSE-trained networks are therefore systematically biased at low effective SNR for ADC and IVIM diffusion coefficients.

The relatively higher accuracy of the NLR loss for diffusion coefficient estimation at low SNR (Fig. 3) is explained by its ability to account for the potential skewness of the Rician-distributed measures. Estimation of diffusion coefficients requires accurate estimation of the rate of noise-free signal decay. At high diffusivities or low SNRs, the noise-free signal, and therefore the effective SNR, is lower, resulting

in signal measures that deviate increasingly upwards from the noise-free signal¹⁷ (Fig. 2). Under these conditions, the NLR loss maintains a relatively accurate noise-free signal prediction by optimising the probability of the data given the predicted measurement distribution. However, the MSE loss aims to reduce the residual error on the noise-free signal prediction regardless of the data distribution, ignoring the skewed distribution of measures. This results in MSE underestimating the rate of signal attenuation and underestimating the diffusion coefficient.

Underestimation of diffusion coefficient using MSE-trained networks is consistent with previous studies. Increasing underestimation of IVIM diffusion coefficient D_i with lower SNR, reaching a bias of $-0.4 \mu\text{m}^2/\text{ms}$ at SNR=10, broadly agrees with results from Epstein et al.¹², Barbieri et al.⁴ and Zhou et al.¹¹, who report bias and median errors of -0.4 and $-0.2/-0.5 \mu\text{m}^2/\text{ms}$ at low SNR, respectively. The marginally higher accuracy reported by Barbieri et al.⁴ may be because they quantified accuracy using the median, which is more robust to skewed error distributions, while the lower accuracy reported by Zhou et al.¹¹ may be due to their use of model selection which creates an additional source of variability. The ADC diffusion coefficient D tends to have higher accuracy than the IVIM diffusion coefficient D_i , likely because ADC is a simpler model with a higher number of measurements per parameter.

For both losses, IVIM D_p and f parameters show overestimation that worsens at low effective SNR. This may be explained by the degenerate nature of the IVIM model:- a reduction (underestimation) of D_i , which leads to less predicted signal attenuation, can be offset by an increase in D_p or f .

The NLR loss marginally overestimated the ADC diffusion coefficient at low effective SNRs, reaching a bias of around 1% at high SNR. This may be explained by the shallow gradient of the likelihood function at high diffusivities – the value of D has less impact on the predicted signal at higher values. This means that, with finite sample size, small variation in noise instantiation can lead to relatively large increases in the MLE, thus creating a skewed and hence biased MLE distribution. Quantile-based analysis in Fig. 5 shows that the median error remains close to zero for D even at very low SNR, despite the overestimation bias indicated by Fig. 3 and 4. It should also be noted that while MLE is known to be asymptotically unbiased, finite sample sizes can be a source of bias in non-linear model parameter estimation³⁶. Extending the NLR loss to account for the posterior probability of parameter estimates given a prior distribution may mitigate this problem and is the topic of current research.

The proposed loss has wide potential application for improving the accuracy of deep-learning based qMRI, as many techniques utilise experimentally attenuated signal measures with low effective SNR. This is the case for diffusion

MR imaging³⁷, relaxometry³⁸, magnetisation transfer imaging³⁹, oxygen imaging⁴⁰, and others. In these cases, low effective SNR data can arise due to a variety of factors, including the biophysical tissue properties of imaged anatomy, the required image resolution, and the choice of acquisition parameters. Biophysical tissue properties that result in high signal attenuation will generate data with low effective SNR. An example of this is diffusion MR imaging in brain cerebrospinal fluid and along coherent white matter tracts. Higher spatial resolution is required to image small-scale anatomical features, producing data with lower SNR, for example in the spinal cord⁴¹ and cerebellum⁴². Furthermore, the acquisition parameters may be customised for a specific model and require highly attenuated signals, as is the case for diffusion kurtosis imaging⁴³. MR experimental choices aimed at increasing SNR to improve the robustness of parameter estimates using MSE-trained networks may now instead consider achieving the same accuracy using the NLR loss.

The proposed loss also has potential application outside of qMRI. It may be utilised for machine learning applications involving MR imaging of nuclei that are relatively less abundant than protons, which therefore produce low SNR data, as is the case in sodium imaging⁴⁴. There is also potential application to prediction tasks requiring batch-based optimisation from Rician-distributed data. For example, for deep learning-based MR image de-noising and synthetic image generation.

6 | CONCLUSIONS

This work proposes and evaluates a numerically stable and accurate negative log Rician likelihood loss function for self-supervised learning in qMRI and compares its performance against the MSE. The NLR loss shows higher parameter estimation accuracy for lower effective SNR data compared to the MSE for ADC and IVIM diffusion coefficients. This has the potential to enable faster and more reliable quantitative analysis in noisy MR datasets, with broad application both within qMRI and beyond.

DATA AVAILABILITY

A tutorial demonstrating the self-supervised training with negative log Rician likelihood loss, as well as PyTorch, Keras and TensorFlow implementations, is available at https://github.com/csparker/deep_qmri.

ACKNOWLEDGMENTS

CSP, DCA and HZ are supported by the Medical Research Council (MR/T046473/1). AS is supported by the EPSRC funded i4health CDT (EP/S021930/1). SCE is supported by the EPSRC-funded UCL Centre for Doctoral Training in Medical Imaging (EP/L016478/1).

Financial disclosure

None.

Conflict of interest

The authors declare no potential conflict of interests.

ORCID

Christopher S. Parker¹  0000-0002-1616-2886

Anna Schroder¹  0009-0001-0380-0674

Sean C. Epstein¹  0000-0002-8071-1114

James Cole¹  0000-0003-1908-5588

Daniel C. Alexander¹  0000-0003-2439-350X

Hui Zhang¹  0000-0002-5426-2140

REFERENCES

- Mara Cercignani, Nicholas G Dowell, and Paul S Tofts. *Quantitative MRI of the brain: principles of physical measurement*. Taylor & Francis, 2018.
- Nicole Seiberlich, Vikas Gulani, Adrienne Campbell-Washburn, Steven Sourbron, Mariya Ivanova Doneva, Fernando Calamante, and Houchun Harry Hu. *Quantitative magnetic resonance imaging*. Academic Press, 2020.
- Vladimir Golkov, Alexey Dosovitskiy, Jonathan I Sperl, Marion I Menzel, Michael Czisch, Philipp Sämann, Thomas Brox, and Daniel Cremers. Q-space deep learning: twelve-fold shorter and model-free diffusion mri scans. *IEEE transactions on medical imaging*, 35(5): 1344–1351, 2016.
- Sebastiano Barbieri, Oliver J Gurney-Champion, Remy Klaassen, and Harriet C Thoeny. Deep learning how to fit an intravoxel incoherent motion model to diffusion-weighted mri. *Magnetic resonance in medicine*, 83(1):312–321, 2020.
- Misha PT Kaandorp, Sebastiano Barbieri, Remy Klaassen, Hanneke WM van Laarhoven, Hans Crezee, Peter T While, Aart J Nederveen, and Oliver J Gurney-Champion. Improved unsupervised physics-informed deep learning for intravoxel incoherent motion modeling and evaluation in pancreatic cancer patients. *Magnetic resonance in medicine*, 86(4):2250–2265, 2021.
- Francesco Grussu, Marco Battiston, Marco Palombo, Torben Schneider, Claudia AM Gandini Wheeler-Kingshott, and Daniel C Alexander. Deep learning model fitting for diffusion-relaxometry: a comparative study. In *Computational Diffusion MRI: International MICCAI Workshop, Lima, Peru, October 2020*, pages 159–172. Springer, 2021.
- Serge Didenko Vasylechko, Simon K Warfield, Onur Afacan, and Sila Kurugol. Self-supervised ivim dwi parameter estimation with a physics based forward model. *Magnetic resonance in medicine*, 87(2):904–914, 2022.
- Tim Ottens, Sebastiano Barbieri, Matthew R Orton, Remy Klaassen, Hanneke WM van Laarhoven, Hans Crezee, Aart J Nederveen, Xiantong Zhen, and Oliver J Gurney-Champion. Deep learning dce-mri parameter estimation: Application in pancreatic cancer. *Medical Image Analysis*, 80:102512, 2022.
- Elisa Scalco, Giovanna Rizzo, and Alfonso Mastropietro. The quantification of intravoxel incoherent motion-mri maps cannot preserve texture information: An evaluation based on simulated and in-vivo images. *Computers in Biology and Medicine*, 154:106495, 2023.
- Noemi G Gyori, Marco Palombo, Christopher A Clark, Hui Zhang, and Daniel C Alexander. Training data distribution significantly impacts the estimation of tissue microstructure with machine learning. *Magnetic resonance in medicine*, 87(2):932–947, 2022.
- Xin-Xiang Zhou, Xin-Yu Wang, En-Hui Liu, Lan Zhang, Hong-Xia Zhang, Xiu-Shi Zhang, Yue-Min Zhu, and Zi-Xiang Kuai. An unsupervised deep learning approach for dynamic-exponential intravoxel incoherent motion mri modeling and parameter estimation in the liver. *Journal of Magnetic Resonance Imaging*, 56(3):848–859, 2022.
- Sean C Epstein, Timothy JP Bray, Margaret Hall-Craggs, and Hui Zhang. Choice of training label matters: how to best use deep learning for quantitative mri parameter estimation. *arXiv preprint arXiv:2205.05587*, 2022.
- Dor Bank, Noam Koenigstein, and Raja Giryes. Autoencoders. *arXiv preprint arXiv:2003.05991*, 2020.
- Robert I Jennrich. Asymptotic properties of non-linear least squares estimators. *The Annals of Mathematical Statistics*, 40(2):633–643, 1969.
- Steven M Kay. *Fundamentals of statistical signal processing: estimation theory*. Prentice-Hall, Inc., 1993.
- Joel Tellinghuisen. Least squares with non-normal data: Estimating experimental variance functions. *Analyst*, 133(2):161–166, 2008.
- Hákon Gudbjartsson and Samuel Patz. The rician distribution of noisy mri data. *Magnetic resonance in medicine*, 34(6):910–914, 1995.
- A Van den Bos. *Handbook of measurement science*, volume 1. Wiley, 1982.
- Jan Sijbers, Arnold J Den Dekker, Paul Scheunders, and Dirk Van Dyck. Maximum-likelihood estimation of rician distribution parameters. *IEEE Transactions on Medical Imaging*, 17(3): 357–361, 1998.
- Ivor JA Simpson, Balázs Örszik, Neil Harrison, Iris Asllani, and Mara Cercignani. Motion correction in low snr mri using an approximate rician log-likelihood. In *International Workshop on Biomedical Image Registration*, pages 147–155. Springer, 2022.
- Patrick J Bolan, Sara L Saunders, Kendrick Kay, Mitchell Gross, Mehmet Akcakaya, and Gregory J Metzger. Improved quantitative

- parameter estimation for prostate t2 relaxometry using convolutional neural networks. *medRxiv preprint medRxiv:2023.01.11.23284194*, pages 2023–01, 2023.
22. Kevin P Murphy. *Probabilistic machine learning: an introduction*. MIT press, 2022.
 23. Milton Abramowitz and Irene A Stegun. Bessel functions of integer order. *Handbook of Mathematical Functions*. Dover Publications, New York, 377, 1972.
 24. Jesper LR Andersson. Maximum a posteriori estimation of diffusion tensor parameters using a rician noise model: why, how and but. *Neuroimage*, 42(4):1340–1356, 2008.
 25. Cephes mathematical functions library. <http://www.netlib.org/cephes/>. Accessed: 2023-07-11.
 26. Donald E Amos. Subroutine package for bessel functions of a complex argument and nonnegative order. Technical report, Sandia National Labs., Albuquerque, NM (USA), 1985.
 27. JM Blair and CA Edwards. Stable rational minimax approximations to the modified bessel functions $i_0(x)$ and $i_1(x)$. Technical report, Atomic Energy of Canada Ltd., 1974.
 28. JM Blair. Rational chebyshev approximations for the modified bessel functions $i_0(x)$ and $i_1(x)$. *mathematics of computation*, 28(126):581–583, 1974.
 29. Denis Le Bihan, Eric Breton, Denis Lallemand, Marie-Louise Aubin, Jean Vignaud, and Maurice Laval-Jeantet. Separation of diffusion and perfusion in intravoxel incoherent motion mr imaging. *Radiology*, 168(2):497–505, 1988.
 30. Denis Le Bihan, Eric Breton, Denis Lallemand, Philippe Grenier, Emmanuel Cabanis, and Maurice Laval-Jeantet. Mr imaging of intravoxel incoherent motions: application to diffusion and perfusion in neurologic disorders. *Radiology*, 161(2):401–407, 1986.
 31. Djork-Arné Clevert, Thomas Unterthiner, and Sepp Hochreiter. Fast and accurate deep network learning by exponential linear units (elus). *arXiv preprint arXiv:1511.07289*, 2015.
 32. Jan Sijbers, Arnold J den Dekker, Erik Raman, and Dirk Van Dyck. Parameter estimation from magnitude mr images. *International Journal of imaging systems and technology*, 10(2):109–114, 1999.
 33. Jan Sijbers, Dirk Poot, Arnold J den Dekker, and Wouter Pintjens. Automatic estimation of the noise variance from the histogram of a magnetic resonance image. *Physics in Medicine & Biology*, 52(5):1335, 2007.
 34. Jeny Rajan, Dirk Poot, Jaber Juntu, and Jan Sijbers. Noise measurement from magnitude mri using local estimates of variance and skewness. *Physics in medicine & biology*, 55(16):N441, 2010.
 35. Diederik P Kingma and Jimmy Ba. Adam: A method for stochastic optimization. *arXiv preprint arXiv:1412.6980*, 2014.
 36. Paul Rilstone, Virendra K Srivastava, and Aman Ullah. The second-order bias and mean squared error of nonlinear estimators. *Journal of Econometrics*, 75(2):369–395, 1996.
 37. Daniel C Alexander, Tim B Dyrby, Markus Nilsson, and Hui Zhang. Imaging brain microstructure with diffusion mri: practicality and applications. *NMR in Biomedicine*, 32(4):e3841, 2019.
 38. Hai-Ling Margaret Cheng, Nikola Stikov, Nilesh R Ghugre, and Graham A Wright. Practical medical applications of quantitative mr relaxometry. *Journal of Magnetic Resonance Imaging*, 36(4):805–824, 2012.
 39. Gunther Helms, Henning Dathe, Kai Kallenberg, and Peter Dechent. High-resolution maps of magnetization transfer with inherent correction for rf inhomogeneity and t1 relaxation obtained from 3d flash mri. *Magnetic Resonance in Medicine: An Official Journal of the International Society for Magnetic Resonance in Medicine*, 60(6):1396–1407, 2008.
 40. Thomas Christen, Pierre Bouzat, Nicolas Pannetier, Nicolas Coquery, Anaïck Moisan, Benjamin Lemasson, Sébastien Thomas, Emmanuelle Grillon, Olivier Detante, Chantal Rémy, et al. Tissue oxygen saturation mapping with magnetic resonance imaging. *Journal of Cerebral Blood Flow & Metabolism*, 34(9):1550–1557, 2014.
 41. CA Wheeler-Kingshott, Patrick W Stroman, JM Schwab, M Bacon, Rachel Bosma, J Brooks, DW Cadotte, Thomas Carlstedt, Olga Ciccarelli, Julien Cohen-Adad, et al. The current state-of-the-art of spinal cord imaging: applications. *Neuroimage*, 84:1082–1093, 2014.
 42. Gaku Okugawa, Kenji Nobuhara, Tatsuya Sugimoto, and Toshihiko Kinoshita. Diffusion tensor imaging study of the middle cerebellar peduncles in patients with schizophrenia. *The Cerebellum*, 4:123–127, 2005.
 43. Jens H Jensen, Joseph A Helpert, Anita Ramani, Hanzhang Lu, and Kyle Kaczynski. Diffusional kurtosis imaging: the quantification of non-gaussian water diffusion by means of magnetic resonance imaging. *Magnetic Resonance in Medicine: An Official Journal of the International Society for Magnetic Resonance in Medicine*, 53(6):1432–1440, 2005.
 44. Guillaume Madelin and Ravinder R Regatte. Biomedical applications of sodium mri in vivo. *Journal of Magnetic Resonance Imaging*, 38(3):511–529, 2013.

SUPPORTING INFORMATION

	$I_0(x)$	$\log(I_0(x))$
Series ²⁰	$\sum_{k=0}^{50} \frac{1}{4} \frac{(x^2)^k}{(k!)^2}$	$\log\left(\sum_{k=0}^{50} \frac{\exp(-k\log(4) + 2k\log(x))}{-2\log\Gamma(k+1)}\right)$
Hankel-1 ²³	$\frac{e^x}{\sqrt{2\pi x}}$	$x - \frac{\log(2\pi x)}{2}$
Hankel-2 ²⁴	e^x	x
Proposed ²⁸	$e^x \sum_{i=0}^{30} c_i^{(l)} T_i(x_t), x = [0,8]$ $\frac{e^x}{\sqrt{x}} \sum_{i=0}^{25} c_i^{(h)} T_i(x_t), x = (8, \infty)$	$x + \log\left(\sum_{i=0}^{30} c_i^{(l)} T_i(x_t)\right), x = [0,8]$ $x + \log\left(\sum_{i=0}^{25} c_i^{(l)} T_i(x_t)\right) - \frac{\log(x)}{2}, x = (8, \infty)$

TABLE S1. Approximate modified Bessel functions of the first kind with order zero and their logarithms. $T_i(x_t)$ are Chebyshev polynomials of the first kind evaluated at x transformed to the range $[-1,1]$ and c_i^* are vectors of coefficients for the low or high ranges of x .

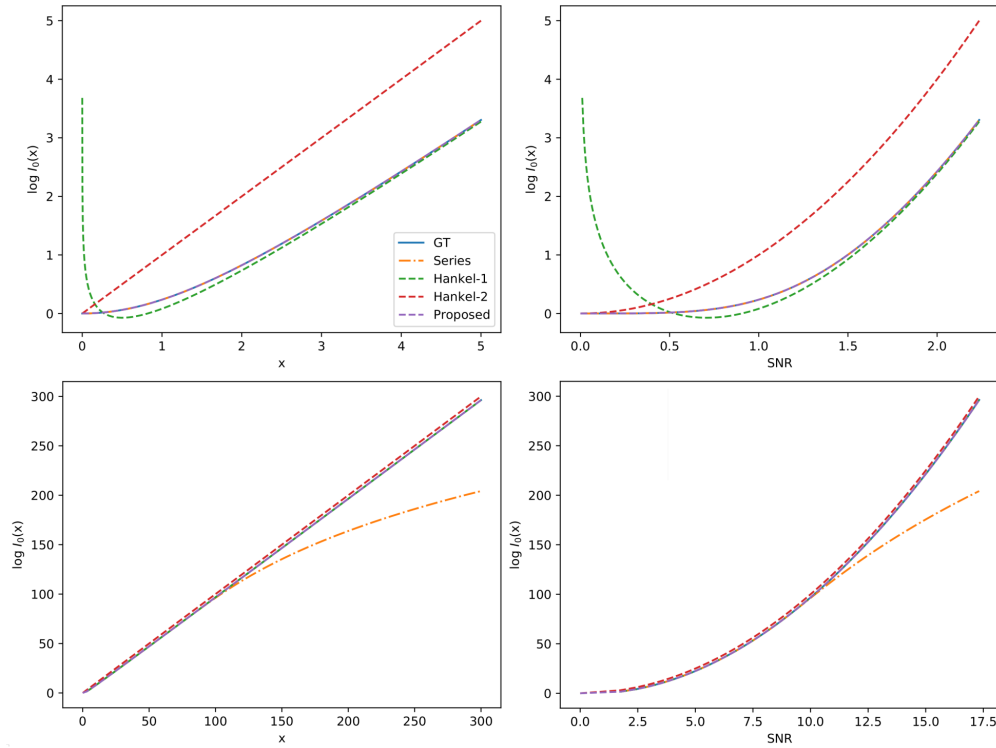


FIGURE S1. $\log(I_0(x))$ approximations as a function of input, x , and $\text{SNR} \approx \sqrt{x}$. In the left column, plots are a function of x . In the right column, plots are a function of SNR. The top and bottom rows show different ranges of SNRs - low and high, respectively. The ground truth (GT, blue line) was computed using 1000 summations of the series expansion, which converges in value for the range of x shown. Note the GT line is only partially visible as it overlaps with the approximations. In the bottom left plot (high SNR as a function of x), it is fully obscured by the Proposed and Hankel-1 lines.

	Stable training SNRs
Series	[5, 40]
Hankel-1	[10, 40]
Hankel-2	(0, 40]
Proposed	(0,40]

TABLE S2. Range of training data SNRs over which the loss functions incorporating the $\log(I_0(x))$ approximations were numerically stable. Networks were trained on data with SNRs of (0, 40] in increments of 2.5. Training was stable if the loss function did not underflow or overflow. Proposed and Hankel-2 were stable across the entire SNR range, whereas Series and Hankel-1 were unstable at low SNR.

How to cite this article: C.S. Parker., A Schroder, S.C. Epstein, J. Cole, D.C. Alexander, and H. Zhang (2023), Rician likelihood loss for quantitative MRI using self-supervised deep learning, *arXiv*.